Electronic Supplementary Material (ESI) for Journal of Materials Chemistry A.

Supporting Information for Machine-Learning Assisted High-Throughput Discovery of Solid-State Electrolytes for Li-ion Batteries

Xingyu Guo,[*,†] Zhenbin Wang,[‡,¶] Ji-Hui Yang,[†] and Xin-Gao Gong[*,†]

†*Department of Physics, Key Laboratory of Computational Physical Sciences (Ministry of Education), Institute of Computational Physical Sciences, State Key Laboratory of Surface Physics, Fudan University, Shanghai 200433, China*

‡*Department of Materials Science and Engineering, City University of Hong Kong, Hong Kong 999077, China*

¶*School of Energy and Environment, Department of Materials Science and Engineering, City University of Hong Kong, Hong Kong 999077, China*

E-mail: xguo@fudan.edu.cn; xggong@fudan.edu.cn

Li^+ conductivity of known lithium-ion conductors

Table S1: Li^+ conductivity of selected known lithium-ion conductors.

Material	Exp. (mS/cm)	Ref
$Li_4P_2S_6$	2.38 x 10^{-4}	[1]
$LiZnPS_4$	$\sim 10^{-4}$	[2]
$Li_{10}GeP_2S_{12}$	12	[3]
$Li_{10}SiP_2S_{12}$	2.3	[4]
$Li_{10}SnP_2S_{12}$	4	[5]
$Li_7P_3S_{11}$	1.5	[6]
$Li_{10}Si_{1.5}P_{1.5}S_{11.5}Cl_{0.5}$	25	[7]
Li_6PS_5Cl	3.15	[8]
$Li_7La_3Zr_2O_{12}$ (LLZO)	$\sim 10^{-1}$	[9]
$Li_2La_2Ti_3O_{10}$ (LLTO)	$\sim 10^{-2}$	[10]
$Li_3OCl_{0.5}Br_{0.5}$	~ 1	[11]
Li_3YCl_6	0.51	[12]
Li_3YBr_6	1.70	[12]
$LiFePO_4$	$10^{-8} \sim 10^{-7}$	[13,14]
NCM111	$10^{-2} \sim 10^{-3}$	[15]
$LiCoO_2$	$10^{-2} \sim 1$	[16–18]

Benchmark of electronic band gaps

Table S2: Calculated band gaps of common solid-state electrolytes, obtained from density functional theory (DFT) calculations, using the Perdew–Burke–Ernzerhof (PBE) and Heyd–Scuseria–Ernzerhof (HSE) functionals, and machine-learning (ML) predictions using the HSE 4-fi-MEGNet model.

material	E_g (eV)		
	DFT-PBE	DFT-HSE	ML-HSE
c−Na_3PS_4	2.29	3.38	3.17
$LiZnPS_4$	2.73	3.86	3.69
$LiAl(PS_3)_2$	2.75	3.74	3.58
$Li_4P_2S_6$	0	-	3.27
$Li_{10}GeP_2S_{12}$	2.06	-	3.14
$Li_{10}SiP_2S_{12}$	2.38	-	3.54
$Li_{10}SnP_2S_{12}$	2.0	-	3.16
$Li_7P_3S_{11}$	2.41	-	3.44
$Li_5PS_4Cl_2$	2.78	3.57	3.57
$Li_{10}Si_{1.5}P_{1.5}S_{11.5}Cl_{0.5}$	2.31	-	3.56
Li_3PS_4	2.81	-	3.44
$Li_7La_3Zr_2O_{12}$ (LLZO)	4.33	4.12	5.43
$Li_2La_2Ti_3O_{10}$ (LLTO)	2.84	3.34	3.33

Statistics of screening process

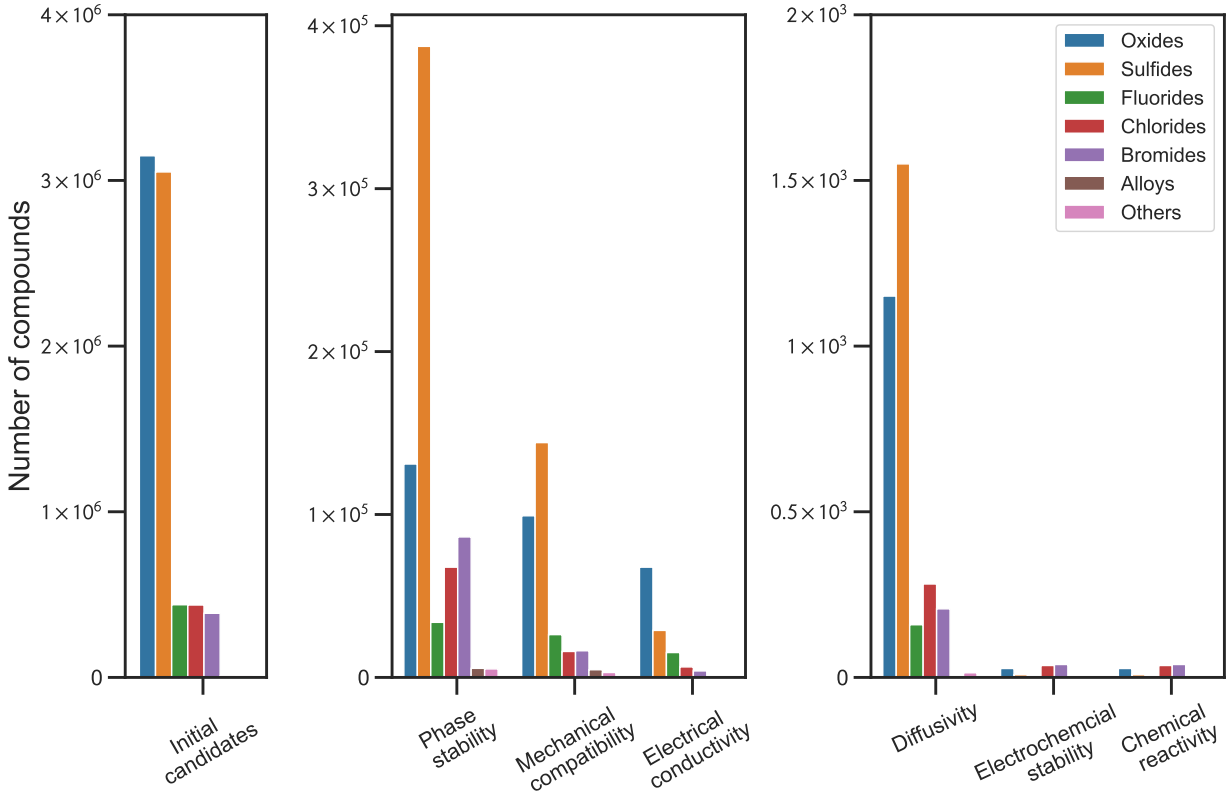

Figure S1: Histogram of numbers of compounds for each category that pass each filter in the high-throughput identification.

Table S3: Statistical analysis of lithium-based compounds from the Inorganic Crystal Structure Database(ICSD), Materials Project and Mattaverse database. This analysis quantifies the materials from the Materials Project and Mattaverse database that meet the phase stability screening criterion, defined as energy above the hull (E_{hull-m}) being less than 30 meV/atom. The analysis was limited to ordered structures only.

	ICSD	Materials Project	Mattaverse
Oxides	1,497	3,258	13,097
Sulfides	110	206	38,735
Fluorides	157	320	3,382
Chlorides	47	98	6,767
Bromides	29	47	8,624
Alloys	260	756	556
Others	789	594	448

Tree-based Classification Model on Li^+ conductivities

Leveraging the dataset (10,769 data point) produced in our high-throughput calculations, we developed a machine learning tree-based classification model to elucidate the structure-chemistry-conductivity relationship. According to our benchmark results, solid electrolytes with an $MSD_{800K} > 5$ Å^2 demonstrate baseline Li^+ conductivities. We thus classified the candidates into two groups : materials with MSD_{800K} below 5 Å^2 are designated as having no Li^+ conduction (Probability of Li^+ conduction = 0), while materials with MSD_{800K} exceeding 5 Å^2 are identified as dispalying baseline Li^+ conductivity (Probability of Li^+ conduction = 1).

87 physically-informed features were created for each material to describe their properties of composition, crystal structure and crystal sites. For example, the channel size of Li^+ is characterized by the maximum packing efficiency, the packing fraction and volume of the given material. Maximum packing efficiency is defined as the maximum spatial occupancy of an atom within its local environment in a crystal structure. This efficiency is quantified by $\sum_N \frac{4}{3} \cdot \pi \cdot r_{max}^3$, where V represents the volume of the structure, N is the number of sites in the structure, and r_{max} is the radius of the largest possible atom for each site. The value of r_{max} is determined by the distance from the center of the cell to the nearest Voronoi face.[19] The packing fraction evaluates the ratio of the volume occupied by atoms to the total crystal lattice volume, calculated as $\sum_N \frac{4}{3} \cdot \pi \cdot r_{atomic}^3$, with r_{atomic} denoting the atomic radius of each atom in the structure. The connectivity of the channel size for Li^+ within a structure is derived from its volume and packing fraction. A higher packing fraction indicates less void space within the structure, potentially decreasing the connectivity of Li^+ conduction channels. In contrast, a larger volume suggests more void space, implying enhanced connectivity for Li^+ conduction channels.

For features exhibiting a high degree of correlation with one another—specifically, those with a Pearson correlation coefficient greater than 0.75—the feature yielding better perfor-

mance was selected to construct the model, as shown in Figure S2. The developed classification model demonstrates an accuracy score of 0.975 and a Jaccard score of 0.962, indicating its high accuracy in distinguishing Li^+ baseline conductivities.

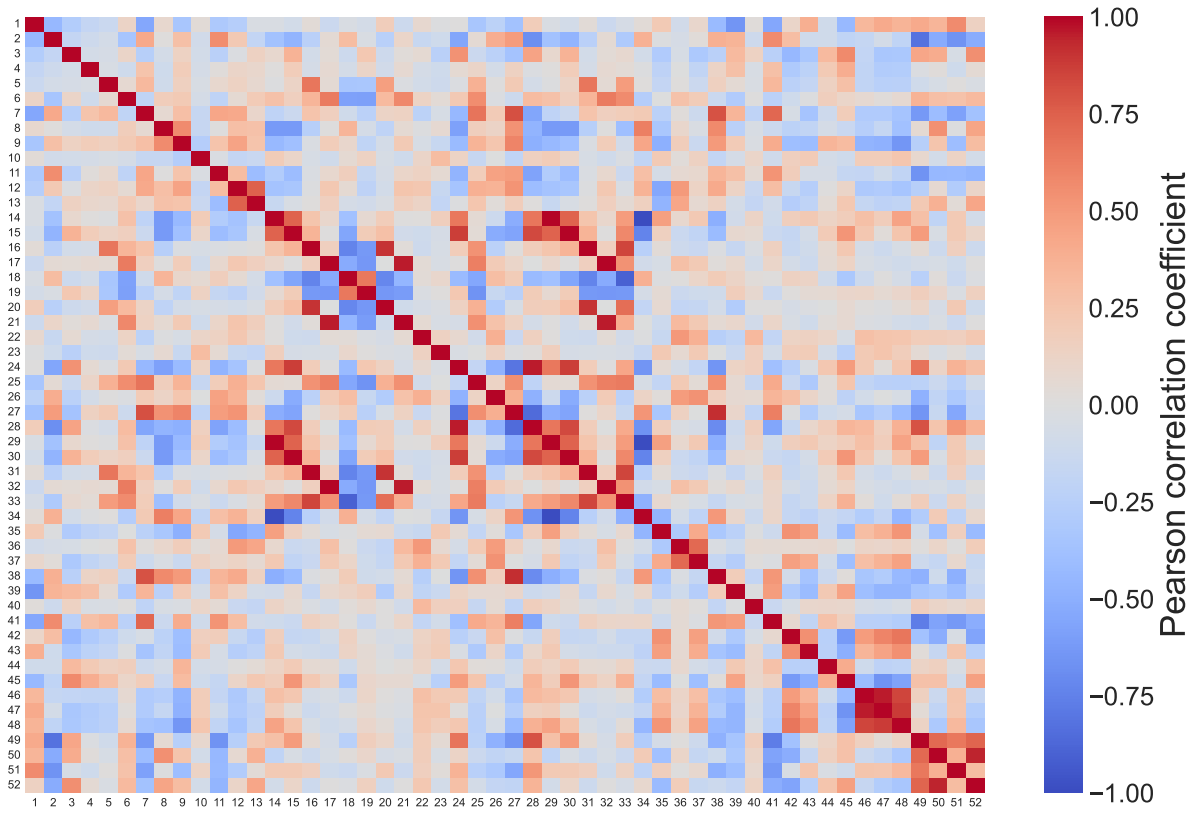

Figure S2: Calculated Pearson correlation coefficients of the pairs of features. The features are 1.Li-O bond fraction; 2.Li-S bond fraction; 3.Li-F bond fraction; 4.Li-Cl bond fraction; 5.Li-Br bond fraction; 6.Density; 7.Volume per atom; 8.Packing fraction; 9.Maximum packing efficiency; 10.Structural complexity per cell; 11.HOMO energy; 12.LUMO energy; 13.Atomic orbitals; 14.Average number of s valence electrons; 15.Average number of p valence electrons; 16.Average number of d valence electrons; 17.Average number of f valence electrons; 18.Fraction of s valence electrons; 19.Fraction of p valence electrons; 20.Fraction of d valence electrons; 21.Fraction of f valence electrons; 22.Transition metal fraction; 23.Stoichiometry 0-norm; 24.Band center; 25.MagpieData mean atomic weight; 26.Mean melting T; 27.Mean covalent radius; 28.Mean electronegativity; 29.Mean number of s valence electrons; 30.Mean number of p valence electrons; 31.Mean number of d valence electrons; 32.Mean number of f valence electrons; 33.Mean number of valence electrons; 34.Mean number of unfilled s orbitals; 35.Mean number of unfilled p orbitals;; 36.Mean number of unfilled d orbitals;; 37.Mean number of unfilled orbitals; 38.Ground state volume per atom; 39.Mean ground state bandgap; 40.Mean ground state magmom; 41.Average bond length Li-X; 42.Mean Li interstice area; 43.Mean Li interstice volume; 44.Coordination number; 45.Minimum oxidation state; 46.Maximum oxidation state; 47.Range of oxidation state; 48.Standard deviation of oxidation state; 49.Maximum ionic charge; 50.Average ionic charge; 51.Average anion electron affinity; 52.Mean electronegativity difference

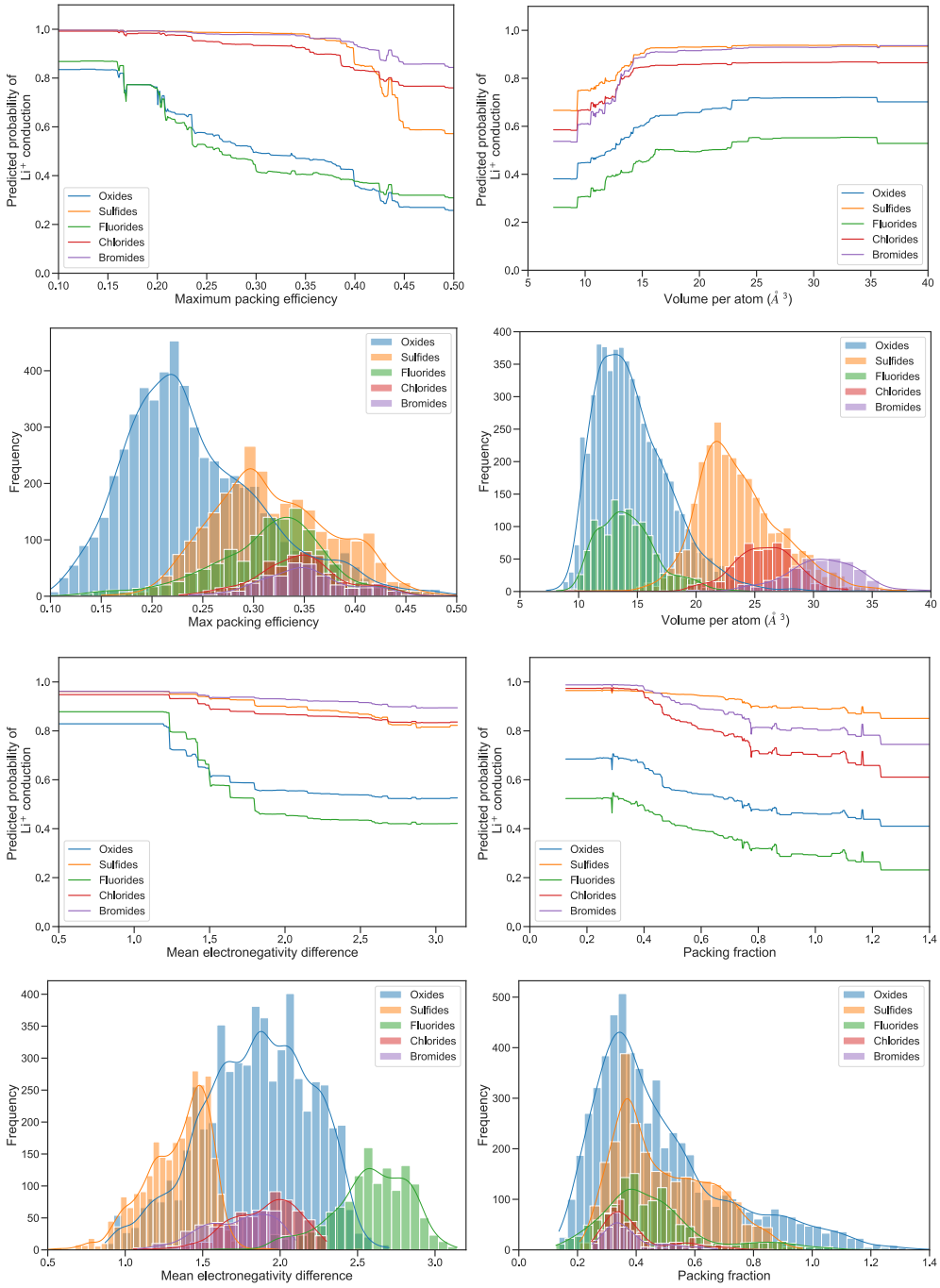

Figure S3: Partial dependence plots illustrating the influence of different features, (a) Maximum packing efficiency, (b) Packing fraction, (c) Volume per atom, and (d) Electronegativity difference, on the classification of Li^+ diffusions. The accompanying histogram displays the frequency distribution of the datasets according to the feature values.

According to Figure S3, it is found that sulfides have in general larger volume than oxides and fluorides, suggesting that sulfides are more likely to form connected Li^+ diffusion channels. Meanwhile, sulfides exhibit the smallest mean electronegativity difference with respect to Li, indicating minimized interactions of Li^+ with neighboring anions while hopping. Similarly, chlorides and bromides also tend to form crystals with large volumes, enabling fast Li^+ transportation. In contrast, oxides and fluorides tend to form crystals with relatively small volume, which may reduce the connection between individual Li^+ diffusion channels. The large mean electronegativity difference in fluorides may result in sluggish Li^+ diffusion. Therefore, the likelihood of finding fast Li^+ conductors is higher in sulfides, chlorides, and bromides than it is in oxides and fluorides.

Structure prototypes of the 130 identified promising candidate materials.

Table S4: Structure prototypes for the 130 promising candidate materials for solid electrolytes are represented in two ways: (i) the parent structure from which the candidate materials are derived through substitution; and (ii) the structure type of the parent structure as listed in the Inorganic Crystal Structure Database (ICSD).[20,21] The symbol '—' denotes the absence of a structure type in the ICSD.

Promising candidates			Parent Structures		Structure type
Material	Space group	Material ID	Material	ICSD ID	
LiCl	P6_3mc(186)	mp-1185319	LiCl	-	-
LiBr		mv-25910967	LiBr		
$Cs_2LiScCl_6$	Fm-3m(225)	mp-1113004	$Cs_2LiScCl_6$	-	-
$SrLi_2SiO_4$	Pnma(62)	mv-25910959	Li_2CdSiO_4	1113	Li_3PO_4
$SrLi_2GeO_4$		mv-25910967			
$SrLiLuCl_6$	P2_1/m(11)	mv-23258662	$KHoBeF_6$	2143	-
$LiLuCl_4$	P2_12_12_1(19)	mv-31579856	$NaAlCl_4$	2307	$NaAlCl_4$
$SrLiScCl_6$	P321(150)	mv-23989007	$LiMgAlF_6$	5007	Na_2SiF_6
$SrLiScBr_6$		mv-23989008			
$SrLiLuBr_6$		mv-23989089			
$BaLiLuCl_6$		mv-23989643			
$SrLiLuCl_6$		mv-23989088			
Li_2BeF_4	I-4(82)	mv-5203013	Ag_2HgI_4	6069	$CdAl_2S_4$#$CdGa_2S_4$
Rb_2LiYBr_6	P-3m1(164)	mv-28307133	Cs_2LiGaF_6	9004	-
$NaLi_2LuBr_6$		mv-28300644			
$K_2LiScBr_6$		mv-28304448			
LiH_3O_2	C2/m(12)	mp-27281	LiH_3O_2	9138	$LiOHH_2O$
$LiLu_2Cl_7$	C2/c(15)	mv-19344575	$CsSb_2F_7$	14119	$CsSb_2F_7$
$LiAl_2F_7$		mv-19344508			
$Li_4Ca_2Si_3O_{10}$	C2/c(15)	mv-13090933	$Na_4Cd_2Si_3O_{10}$	20185	$Na_4Cd_2Si_3O_{10}$
$Rb_3LiCaBr_6$	R-3m(166)	mv-16033288	$K_3NaFeCl_6$	23182	K_4CdCl_6
$LiB(HO)_4$	Pbca(61)	mp-23662	$LiB(HO)_4$	23837	$LiB(OH)_4$

Table S4: Continued

Promising candidates			Parent Structures		Structure type
Material	Space group	Material ID	Material	ICSD ID	
$LiLuCl_4$	P2_1/c(14)	mv-31586317	$NaSbF_4$	24750	$LaTaO_4$
$CsLiCl_2$	Cmcm(63)	mv-31595624	$RbLiBr_2$	30719	RbLiBr2
$KLiCl_2$		mv-31595564			
$KLi_7(SiO_4)_2$	C2/m(12)	mv-8803250	$RbLi_7(SiO_4)_2$	33864	-
$Rb_7LiHf_2O_8$		mv-8805837			
$NaLi_7(GeO_4)_2$		mv-8803210			
$KLi_7(GeO_4)_2$		mv-8803254			
$LiLuCl_4$	P2/c(13)	mv-31568835	$LiAuF_4$	33953	-
$K_2LiLuBr_6$	Pa-3(205)	mv-28933317	K_2NaAlF_6	34201	Ba_2CrUO_6
Li_3ScCl_6	Pna2_1(33)	mv-22830798	Li_3AlF_6	34672	-
Li_3LuCl_6		mv-22830879			
K_3LiSiS_4	P2_1/c(14)	mv-15996940	Rb_3NaPbO_4	35416	Rb_3NaTiO_4
$SrLiScBr_6$	P6_322(182)	mv-24115725	$LiSmAlF_6$	36538	$LiSmAlF_6$
$SrLiLuBr_6$		mv-24115806			
$BaLiScCl_6$		mv-24116279			
$BaLiLuCl_6$		mv-24116360			
$LiLu_2Cl_7$	P2_1/c(14)	mv-20883250	KDy_2Cl_7	37007	-
$Li_3Lu_2Br_9$	P321(150)	mv-15922265	$Cs_3As_2Cl_9$	45733	$Cs_3Bi_2Cl_9$(hP14)
$K_5Li(SiS_3)_3$	P2_1/m(11)	mv-15353762	$Cs_5Si_3AgO_9$	51508	-
$RbLi_2Cl_3$	P2_1/m(11)	mv-18416575	$CsCu_2ICl_2$	60960	$SbPO_4$#$SbAsO_4$
$CsLi_2Cl_3$		mv-18417331			
$Rb_5LiBe_8S_{11}$	P-1(2)	mv-15858566	$RbNa_5Be_8O_{11}$	65482	
Li_3LuCl_6	P-31m(162)	mv-23180659	$NbHg_3F_6$	62027	Hg_3NbF_6
Li_3ScBr_6		mv-23179688			
Li_3LuBr_6		mv-23180660			
$LiSc_6Tl_2Br_{21}$	C2(5)	mv-7289445	$Rb_2NaAl_6F_{21}$	68555	-
$Na_2Li(Sc_2Br_7)_3$		mv-7289436			
$NaLi_2(Sc_2Br_7)_3$		mv-7289447			
$Na_2LiLu_6Br_{21}$		mv-7301100			

Table S4: Continued

Promising candidates			Parent Structures		Structure type
Material	Space group	Material ID	Material	ICSD ID	
$NaLi_2Lu_6Br_{21}$		mv-7301111			
$KLi_2(Sc_2Br_7)_3$		mv-7289471			
$Sr_2LiLuCl_8$		mv-26367164			
$Sr_2LiLuBr_8$	P2_1/c(14)	mv-26367165	$NaSr_2CrF_8$	69032	-
$Ba_2LiLuBr_8$		mv-26367720			
$NaLi_2PO_4$	Pnma(62)	mp-558045	$NaLi_2PO_4$	69967	Li_3PO_4
K_2LiTaO_4		mv-26169630			
$NaLiHfF_6$	Pnma(62)	mv-23751362	$KNaSiF_6$	71334	$KNaSiF_6$
$LiScBr_4$	P2_1/c(14)	mv-31583403	$NaMnF_4$	71455	$LiMnF_4$
$SrLiScCl_6$		mv-24237717			
$SrLiScBr_6$	P2_12_12_1(19)	mv-24237718	$NaSrFeF_6$	71577	Nd_2WO_6(oP36)
$BaLiLuCl_6$		mv-24238353			
$BaLiLuBr_6$		mv-24238354			
Rb_4LiNbO_5	P-1(2)	mv-955162	KLi_4NbO_5	73124	-
$Ba_7Li_2Lu_6Cl_{34}$	C2/m(12)	mv-16242402	$Na_2Sr_7Al_6F_{34}$	78488	-
$Sr_7Li_2Lu_6Cl_{34}$		mv-16242397			
$SrLiLuCl_6$	Pnma(62)	mv-24203184	$NaAlCdF_6$	80559	-
$BaLiLuCl_6$		mv-24203199			
$Na_2Li(ScBr_4)_3$		mv-6302369			
$Na_2LiLu_3Br_{12}$	C2/c(15)	mv-6302396	$Cs_2KMn_3F_{12}$	83873	-
$K_2Li(ScBr_4)_3$		mv-6305033			
$Cs_4Li_2Al_4S_9$	P-1(2)	mv-16124360	$K_2Dy_4Cu_4S_9$	97562	$K_2Dy_4Cu_4S_9$
$LiInO_2$	P-1(2)	mv-27283190	$AgCO_2$	109601	$Ag_2C_2O_4$
Li_2HfCl_6	C2/c(15)	mv-28216780	Li_2ZrF_6	155020	-
$SrLiScCl_6$		mv-24018901			
$SrLiLuCl_6$		mv-24018982			
$SrLiScBr_6$	P4_2nm(102)	mv-24018902	$LiMnVF_6$	167073	$LiFe_2F_6$
$SrLiLuBr_6$		mv-24018983			
$LiCaScBr_6$		mv-24017903			

Table S4: Continued

Promising candidates			Parent Structures		Structure type
Material	Space group	Material ID	Material	ICSD ID	
$BaLiLuCl_6$		mv-24019537			
$KLiSiO_3$	Iba2(45)	mv-27371981	$TlAgTeO_3$	169995	-
$SrLi(BO_2)_3$	P-1(2)	mv-17202210	$KZn(BO_2)_3$	174357	$KZnB_3O_6$
$SrLi_2GeO_4$	P2_1/c(14)	mv-25943051	Li_2FeSiO_4	186519	-
Li_2CaBr_4	Ama2(40)	mv-20014595	$Rb_2Cd(IBr)_2$	194236	Sr_2GeSe_4
$LiLu_3F_{10}$	P222_1(17)	mv-8011123	$RbIn_3F_{10}$	200052	-
$Li_2LuBr_2Cl_3$	P-1(2)	mv-5349815	$Rb_2SbCl_3F_2$	200497	-
$LiLuBr_4$	P2_1/c(14)	mv-31587649	$NaSbF_4$	200573	$LiTaO_4$
$LiLuCl_4$	P2_1/c(14)	mv-31635209	$TlSbF_4$	201084	-
Li_2HfF_6	P2_1/c(14)	mv-22716062	K_2TeClF_5	201603	Sn_3BrF_5
Li_2HfClF_5		mv-22716067			
KLi_2ScBr_6	C2/c(15)	mv-28459714	CsK_2BiCl_6	201983	Rb_3YCl_6
$K_2LiLuBr_6$		mv-28471345			
$Rb_5LiZr_2S_7$	C2/c(15)	mv-12207323	$Na_5AgGe_2S_7$	237455	$Na_6Ge_2Se_7$
$LiScBr_4$	C2/c(15)	mv-31284828	$AlTlF_4$	202455	NH_4AlF_4
$LiLuCl_4$		mv-31285788			
$Sr_3Li_2Lu_2Cl_{14}$	I2_13(199)	mv-3242974	$Na_2Ca_3Al_2F_{14}$	202657	-
$Ba_3Li_2Lu_2Cl_{14}$		mv-3243154			
$K_3Li_2F_5$	Fmm2(42)	mv-9126917	$Cs_3Li_2F_5$	245964	-
$Rb_2Li_3Br_5$	Amm2(38)	mv-8407962	$Cs_2Li_3F_5$	245966	-
$Rb_2Li_3Cl_5$		mv-8407950			
$Rb_2Li_3Br_5$	Imm2(44)	mv-7977990	$Cs_2Li_3Cl_5$	245973	-
$RbLi_3Br_4$	Cmcm(63)	mv-22499633	$CsLi_3Cl_4$	245975	-
$SrLiVO_4$	Pnma(62)	mv-30437085	$LiCoPO_4$	258957	Olivine#Mg_2SiO_4
$Na_2Li(ScBr_4)_3$	P2_1/m(11)	mv-6704684	$Cs_2KTi_3F_{12}$	259399	$Cs_2NaTi_3F_{12}$
$NaLi_2Lu_3Br_{12}$		mv-6703544			
$Na_2LiLu_3Br_{12}$		mv-6704765			
$K_2Li(ScBr_4)_3$		mv-6707348			

Table S4: Continued

Promising candidates			Parent Structures		Structure type
Material	Space group	Material ID	Material	ICSD ID	
Cs_2LiPO_4	Fddd(70)	mv-24746431	Cs_2LiVS_4	414186	$K_2CuNbSe_4$
$LiLu_2Cl_7$	P-1(2)	mv-21560230	$TlBi_2Cl_7$	421318	-
$RbLiCl_2$	C2/c(15)	mv-31397981	$CsLiCl_2$	423634	-
$RbLiLuCl_5$	P2_1/c(14)	mv-22089781	$KLiTmF_5$	428536	$LiKYF_5$
$Li_3Ca(BO_2)_5$	P-1(2)	mv-1332650	$Na_3Sr(BO_2)_5$	260005	$Na_3SrB_5O_{10}$
$SrLiLuCl_6$	P2_1/c(14)	mv-8065139	$BaLiAlF_6$	260011	$LiBaCrF_6$
$SrLiScBr_6$		mv-8065059			
$SrLiLuBr_6$		mv-8065140			
$Rb_3Li_4Y_2Cl_{13}$	Pn-3(201)	mv-15830245	$Rb_3Tm_2Cu_4Br_{13}$	402503	-
$Rb_3Li_4Lu_2Cl_{13}$		mv-15830965			
$Li_7Lu_2Cl_{13}$		mv-15824305			
$K_3Li_4Lu_2Cl_{13}$		mv-15828301			
$Cs_3Li_4Lu_2Cl_{13}$		mv-15834961			
$Na_3Li_4Sc_2Br_{13}$		mv-15824666			
$Na_3Li_4Lu_2Br_{13}$		mv-15825638			
$Li_7Lu_2Br_{13}$		mv-15824306			
$K_3Li_4Lu_2Br_{13}$		mv-15828302			
$Cs_3Li_4Al_2Cl_{13}$		mv-15833881			
$Na_3Li_4Sc_2Cl_{13}$		mv-15824665			
$Na_3Li_4Y_2Cl_{13}$		mv-15824917			
$Na_3Li_4Lu_2Cl_{13}$		mv-15825637			
$K_3Li_4Y_2Cl_{13}$		mv-15827581			

Calculated properties of identified promising solid-state electrolytes (σ_{300K} < 10 mS/cm)

Table S5: Calculated properties of identified promising solid-state electrolytes with Li^+ conductivities lower than 10 mS/cm at 300 K. These properties include the composition of candidate material, phase stability (E_{hull-m}), shear modulus (G), Pugh's ratio (G/K), HSE band gap (E_g), electrochemical stability window, Li^+ conductivity at 300 K and material's ID in the Matterverse database. The data is sorted by the predicted E_{hull-m} value. For materials do not exhibit diffusive behaviors in long-time MD simulations at 300 K, their σ_{300K}s were marked as "-".)

Material	E_{hull-m} (meV/atom)	G (GPa)	G/K	E_g (eV)	Electrochemical window (V)	σ_{300K} (mS/cm)	Material ID
K_3LiSiS_4	-187	12.63	0.45	2.96	1.10∼3.56	0.01	mv-15996940
$Cs_4Li_2Al_4S_9$	-166	9.54	0.38	3.05	0.79∼3.64	0.47	mv-16124360
Rb_4LiNbO_5	-115	16.44	0.51	2.82	1.09∼3.67	0.15	mv-955162
$Rb_5LiZr_2S_7$	-110	8.83	0.40	2.53	0.75∼3.25	2.55	mv-12207323
$Rb_5LiBe_8S_{11}$	-95	11.47	0.44	3.22	0.81∼4.11	0.02	mv-15858566
K_2LiTaO_4	-87	11.82	0.41	3.66	0.81∼3.25	-	mv-26169630
$Rb_7LiHf_2O_8$	-70	10.75	0.49	2.53	1.37∼3.82	0.33	mv-8805837
$K_3Li_4Lu_2Br_{13}$	-28	8.86	0.51	3.69	0.62∼3.38	6.23	mv-15828302
$K_2LiLuBr_6$	-16	9.43	0.54	3.54	0.67∼3.39	0.01	mv-28933317
$K_2Li(ScBr_4)_3$	-14	8.47	0.41	2.96	0.89∼3.48	0.04	mv-6305033
$LiSc_6Tl_2Br_{21}$	-13	8.46	0.38	2.95	1.19∼3.32	-	mv-7289445
$K_2LiLuBr_6$	-12	8.70	0.48	2.41	0.68∼3.26	6.06	mv-28471345
$SrLiLuCl_6$	-11	11.23	0.41	4.76	0.70∼4.36	-	mv-23989088
$LiLu_2Cl_7$	-11	8.93	0.54	4.65	0.72∼4.37	1.2	mv-19344575
Li_2HfF_6	-9	9.69	0.32	6.42	1.16∼6.40	0.61	mv-22716062
$K_3Li_4Lu_2Cl_{13}$	-8	10.22	0.47	4.88	0.62∼4.33	0.19	mv-15828301
$K_2LiScBr_6$	-7	9.05	0.57	3.06	0.90∼3.29	-	mv-28304448
$BaLiLuCl_6$	-6	9.33	0.57	4.80	0.72∼4.31	-	mv-24116360
$SrLi_2GeO_4$	-6	37.72	0.60	3.54	1.09∼3.41	0.37	mv-25910967
$BaLiLuCl_6$	-6	9.82	0.41	4.83	0.72∼4.31	2.71	mv-24238353
$SrLiLuCl_6$	-6	10.81	0.40	4.75	0.72∼4.31	-	mv-24018982

Table S5: Continued

Material	E_{hull-m} (meV/atom)	G (GPa)	G/K	E_g (eV)	Electrochemical window (V)	σ_{300K} (mS/cm)	Material ID
$SrLiLuBr_6$	-5	9.47	0.45	4.02	0.71∼3.28	-	mv-23989089
$Rb_3Li_4Lu_2Cl_{13}$	-4	10.17	0.45	5.07	0.67∼4.3	2.99	mv-15830965
$SrLiLuBr_6$	-4	10.04	0.48	4.00	0.71∼3.27	-	mv-24018983
$LiLuCl_4$	-4	8.72	0.38	4.58	0.73∼4.29	-	mv-31285788
$SrLiLuBr_6$	-4	9.86	0.45	3.98	0.71∼3.26	2.89	mv-24115806
$LiLuCl_4$	-3	8.83	0.37	4.56	0.73∼4.28	-	mv-31568835
$LiLuCl_4$	-3	11.00	0.45	4.86	0.73∼4.28	-	mv-31586317
Li_3LuCl_6	-3	13.08	0.48	4.84	0.73∼4.27	3.41	mv-22830879
$BaLiLuBr_6$	-2	8.67	0.41	3.90	0.72∼3.24	-	mv-24238354
$Cs_3Li_4Lu_2Cl_{13}$	-1	9.47	0.46	5.07	0.64∼4.27	5.66	mv-15834961
$Ba_2LiLuBr_8$	0	9.02	0.39	3.96	0.72∼3.23	1.82	mv-26367720
$KLi_2(Sc_2Br_7)_3$	0	8.50	0.41	3.01	0.92∼3.23	0.27	mv-7289471
$SrLi_2GeO_4$	1	36.95	0.58	3.60	1.14∼3.36	-	mv-25943051
$BaLiLuCl_6$	1	9.05	0.44	4.80	0.74∼4.26	-	mv-23989643
$Na_3Li_4Lu_2Br_{13}$	2	11.27	0.60	3.78	0.72∼3.23	4.37	mv-15825638
$LiScBr_4$	2	8.51	0.42	3.06	0.92∼3.23	-	mv-31284828
$LiCaScBr_6$	3	10.64	0.46	3.18	0.92∼3.23	-	mv-24017903
$LiLu_2Cl_7$	5	11.19	0.44	4.03	0.74∼4.26	-	mv-20883250
$Li_2LuBr_2Cl_3$	5	9.78	0.43	4.23	0.74∼3.24	-	mv-5349815
Li_3LuBr_6	5	11.47	0.52	3.86	0.72∼3.23	-	mv-23180660
$SrLiScBr_6$	6	9.00	0.38	3.20	0.92∼3.23	-	mv-23989008
LiH_3O_2	7	16.36	0.57	4.46	1.39∼3.46	-	mp-27281
$SrLiScBr_6$	8	8.84	0.35	3.16	0.92∼3.23	0.2	mv-24115725
$Cs_2LiScCl_6$	8	10.97	0.54	3.71	0.66∼4.3	-	mp-1113004
$NaLi_2PO_4$	9	32.54	0.52	4.98	0.71∼4.01	0.02	mp-558045
$SrLiScBr_6$	9	10.23	0.44	3.21	0.92∼3.23	0.14	mv-24018902
LiBr	9	8.50	0.47	4.33	0.01∼3.23	0.02	mp-976280
Rb_2LiYBr_6	9	8.42	0.56	3.76	0.55∼3.34	0.65	mv-28307133
$BaLiLuCl_6$	9	9.06	0.40	4.79	0.74∼4.26	0.15	mv-24019537

Table S5: Continued

Material	E_{hull-m} (meV/atom)	G (GPa)	G/K	E_g (eV)	Electrochemical window (V)	σ_{300K} (mS/cm)	Material ID
$Na_2LiLu_6Br_{21}$	9	9.68	0.58	3.68	0.72∼3.23	-	mv-7301100
$Rb_3Li_4Y_2Cl_{13}$	10	9.67	0.43	4.69	0.59∼4.26	1.12	mv-15830245
$SrLiScBr_6$	11	10.65	0.43	3.13	0.92∼3.23	-	mv-24237718
$Na_2Li(Sc_2Br_7)_3$	11	10.00	0.51	3.11	0.92∼3.23	-	mv-7289436
Li_3LuCl_6	12	13.68	0.48	4.97	0.74∼4.26	-	mv-23180659
$SrLiLuCl_6$	12	8.92	0.36	4.71	0.74∼4.26	-	mv-23258662
$SrLiLuCl_6$	14	10.72	0.48	4.66	0.74∼4.26	-	mv-8065139
$KLi_7(GeO_4)_2$	14	39.28	0.68	3.93	1.02∼3.35	6.5	mv-8803254
$Sr_2LiLuCl_8$	14	12.55	0.47	4.75	0.74∼4.26	-	mv-26367164
$LiB(HO)_4$	14	18.12	0.53	5.47	1.44∼3.58	-	mp-23662
$NaLi_2(Sc_2Br_7)_3$	14	9.54	0.49	3.04	0.92∼3.23	-	mv-7289447
$CsLi_2Cl_3$	16	9.40	0.59	5.22	0.01∼4.26	-	mv-18417331
$K_3Li_2F_5$	16	22.91	0.56	5.56	0.47∼5.83	5.1	mv-9126917
$SrLiScCl_6$	17	11.54	0.47	3.65	0.92∼4.26	-	mv-23989007
$Sr_2LiLuBr_8$	18	11.22	0.49	3.85	0.72∼3.23	-	mv-26367165
LiCl	18	11.91	0.45	5.80	0.01∼4.26	-	mp-1185319
$SrLiLuBr_6$	18	9.98	0.49	3.80	0.72∼3.23	-	mv-8065140
$Na_2LiLu_3Br_{12}$	19	9.85	0.58	3.80	0.72∼3.23	-	mv-6704765
$LiLuCl_4$	19	9.33	0.53	4.49	0.74∼4.26	-	mv-31579856
$NaLi_2Lu_3Br_{12}$	19	9.44	0.55	3.83	0.72∼3.23	-	mv-6703544
$SrLiScCl_6$	19	11.62	0.49	3.69	0.92∼4.26	3.76	mv-24237717
Li_3ScBr_6	19	12.01	0.54	3.15	0.92∼3.23	-	mv-23179688
$Na_2LiLu_3Br_{12}$	20	9.54	0.57	3.77	0.72∼3.23	-	mv-6302396
Li_3ScCl_6	20	13.36	0.58	3.82	0.92∼4.26	-	mv-22830798
$Cs_3Li_4Al_2Cl_{13}$	20	11.98	0.52	4.19	1.36∼4.26	4.05	mv-15833881
$SrLi_2SiO_4$	21	43.93	0.64	4.36	0.26∼3.48	-	mv-25910959
$NaLi_7(GeO_4)_2$	21	38.09	0.64	3.85	1.02∼3.34	9.45	mv-8803210
$SrLiVO_4$	22	28.34	0.47	3.61	1.42∼3.73	0.01	mv-30437085
$Na_3Li_4Lu_2Cl_{13}$	22	11.69	0.45	4.80	0.62∼3.81	3.71	mv-15825637

Table S5: Continued

Material	E_{hull-m} (meV/atom)	G (GPa)	G/K	E_g (eV)	Electrochemical window (V)	σ_{300K} (mS/cm)	Material ID
$LiInO_2$	22	54.27	0.57	1.80	1.40∼3.24	-	mv-27283190
$Na_2Li(ScBr_4)_3$	23	10.21	0.56	3.14	0.92∼3.23	-	mv-6302369
Li_2HfCl_6	23	10.86	0.60	4.48	1.37∼4.26	4.53	mv-28216780
$RbLiLuCl_5$	23	13.15	0.47	4.46	0.74∼4.26	-	mv-22089781
$NaLiHfF_6$	23	12.77	0.45	6.77	1.18∼6.37	-	mv-23751362
$Na_3Li_4Sc_2Cl_{13}$	24	11.58	0.49	3.92	0.90∼3.81	0.29	mv-15824665
$LiLu_2Cl_7$	24	10.64	0.40	3.99	0.74∼4.26	-	mv-21560230
$Na_3Li_4Y_2Cl_{13}$	24	11.09	0.43	4.62	0.66∼3.81	5.59	mv-15824917
$KLi_7(SiO_4)_2$	25	41.62	0.67	4.60	0.54∼3.38	2.18	mv-8803250
$SrLiScCl_6$	25	11.07	0.46	3.66	0.92∼4.26	0.15	mv-24018901
$SrLi(BO_2)_3$	26	23.04	0.44	4.36	1.25∼3.68	0.2	mv-17202210
$BaLiLuCl_6$	26	9.57	0.41	4.81	0.74∼4.26	-	mv-24203199
$BaLiScCl_6$	26	9.99	0.67	3.70	0.92∼4.26	0.72	mv-24116279
$Na_3Li_4Sc_2Br_{13}$	26	11.12	0.59	3.23	0.92∼3.23	1.06	mv-15824666
$LiLu_3F_{10}$	26	23.30	0.34	6.03	0.73∼6.69	-	mv-8011123
$LiLuCl_4$	26	9.59	0.47	4.68	0.74∼4.26	-	mv-31635209
$LiAl_2F_7$	27	25.42	0.43	7.67	1.29∼6.48	-	mv-19344508
$Li_4Ca_2Si_3O_{10}$	27	36.94	0.55	4.77	0.88∼3.59	1.04	mv-13090933
$KLiSiO_3$	27	34.05	0.68	4.42	0.83∼3.59	-	mv-27371981
$SrLiLuCl_6$	27	10.53	0.44	4.67	0.74∼4.26	-	mv-24203184
$RbLi_2Cl_3$	29	10.95	0.64	5.07	0.01∼4.26	-	mv-18416575
$Li_3Ca(BO_2)_5$	29	30.33	0.5	5.20	1.26∼3.68	-	mv-1332650
Li_2BeF_4	30	16.63	0.41	8.08	0.89∼6.49	-	mv-5203013

References

(1) Hood, Z. D.; Kates, C.; Kirkham, M.; Adhikari, S.; Liang, C.; Holzwarth, N. A. Structural and electrolyte properties of Li4P2S6. *Solid State Ionics* **2016**, *284*, 61–70.

(2) Suzuki, N.; Richards, W. D.; Wang, Y.; Miara, L. J.; Kim, J. C.; Jung, I.-S.; Tsujimura, T.; Ceder, G. Synthesis and Electrochemical Properties of I4-Type Li1+2xZn1-xPS4 Solid Electrolyte. *Chemistry of Materials* **2018**, *30*, 2236–2244.

(3) Kamaya, N.; Homma, K.; Yamakawa, Y.; Hirayama, M.; Kanno, R.; Yonemura, M.; Kamiyama, T.; Kato, Y.; Hama, S.; Kawamoto, K., et al. A lithium superionic conductor. *Nature materials* **2011**, *10*, 682–686.

(4) Whiteley, J. M.; Woo, J. H.; Hu, E.; Nam, K.-W.; Lee, S.-H. Empowering the lithium metal battery through a silicon-based superionic conductor. *Journal of the Electrochemical Society* **2014**, *161*, A1812.

(5) Bron, P.; Johansson, S.; Zick, K.; Schmedt auf der Günne, J.; Dehnen, S.; Roling, B. Li10SnP2S12: an affordable lithium superionic conductor. *Journal of the American Chemical Society* **2013**, *135*, 15694–15697.

(6) Yao, X.; Liu, D.; Wang, C.; Long, P.; Peng, G.; Hu, Y.-S.; Li, H.; Chen, L.; Xu, X. High-energy all-solid-state lithium batteries with ultralong cycle life. *Nano letters* **2016**, *16*, 7148–7154.

(7) Kato, Y.; Hori, S.; Saito, T.; Suzuki, K.; Hirayama, M.; Mitsui, A.; Yonemura, M.; Iba, H.; Kanno, R. High-power all-solid-state batteries using sulfide superionic conductors. *Nature Energy* **2016**, *1*, 1–7.

(8) Wang, S.; Zhang, Y.; Zhang, X.; Liu, T.; Lin, Y.-H.; Shen, Y.; Li, L.; Nan, C.-W. High-conductivity argyrodite Li6PS5Cl solid electrolytes prepared via optimized sintering

processes for all-solid-state lithium–sulfur batteries. *ACS applied materials & interfaces* **2018**, *10*, 42279–42285.

(9) Murugan, R.; Thangadurai, V.; Weppner, W. Fast lithium ion conduction in garnet-type Li7La3Zr2O12. *Angewandte Chemie International Edition* **2007**, *46*, 7778–7781.

(10) Inaguma, Y.; Liquan, C.; Itoh, M.; Nakamura, T.; Uchida, T.; Ikuta, H.; Wakihara, M. High ionic conductivity in lithium lanthanum titanate. *Solid State Communications* **1993**, *86*, 689–693.

(11) Zhao, Y.; Daemen, L. L. Superionic conductivity in lithium-rich anti-perovskites. *Journal of the American Chemical Society* **2012**, *134*, 15042–15047.

(12) Asano, T.; Sakai, A.; Ouchi, S.; Sakaida, M.; Miyazaki, A.; Hasegawa, S. Solid halide electrolytes with high lithium-ion conductivity for application in 4 V class bulk-type all-solid-state batteries. *Advanced Materials* **2018**, *30*, 1803075.

(13) Prosini, P. P.; Lisi, M.; Zane, D.; Pasquali, M. Determination of the chemical diffusion coefficient of lithium in LiFePO4. *Solid state ionics* **2002**, *148*, 45–51.

(14) Xu, Y.-N.; Chung, S.-Y.; Bloking, J. T.; Chiang, Y.-M.; Ching, W. Electronic structure and electrical conductivity of undoped LiFePO4. *Electrochemical and Solid-State Letters* **2004**, *7*, A131.

(15) Li, J.; Liu, Z.; Wang, Y.; Wang, R. Investigation of facial B2O3 surface modification effect on the cycling stability and high-rate capacity of LiNi1/3Co1/3Mn1/3O2 cathode. *Journal of Alloys and Compounds* **2020**, *834*, 155150.

(16) Dokko, K.; Mohamedi, M.; Fujita, Y.; Itoh, T.; Nishizawa, M.; Umeda, M.; Uchida, I. Kinetic characterization of single particles of LiCoO2 by AC impedance and potential step methods. *Journal of the Electrochemical Society* **2001**, *148*, A422.

(17) Barker, J.; Pynenburg, R.; Koksbang, R.; Saidi, M. An electrochemical investigation into the lithium insertion properties of LixCoO2. *Electrochimica acta* **1996**, *41*, 2481–2488.

(18) Levasseur, S.; Ménétrier, M.; Delmas, C. On the dual effect of Mg doping in LiCoO2 and Li1+ δCoO2: structural, electronic properties, and 7Li MAS NMR studies. *Chemistry of materials* **2002**, *14*, 3584–3590.

(19) Ward, L.; Liu, R.; Krishna, A.; Hegde, V. I.; Agrawal, A.; Choudhary, A.; Wolverton, C. Including crystal structure attributes in machine learning models of formation energies via Voronoi tessellations. *Physical Review B* **2017**, *96*, 024104.

(20) Allmann, R.; Hinek, R. The introduction of structure types into the Inorganic Crystal Structure Database ICSD. *Acta Crystallographica Section A: Foundations of Crystallography* **2007**, *63*, 412–417.

(21) Zagorac, D.; Müller, H.; Ruehl, S.; Zagorac, J.; Rehme, S. Recent developments in the Inorganic Crystal Structure Database: theoretical crystal structure data and related features. *Journal of applied crystallography* **2019**, *52*, 918–925.